Modeling of multiple filamentation of terawatt laser pulses on a hundred-meter air path

D.V. Apeksimov[1], Yu.E. Geints[1] , A.A. Zemlyanov[1], A.N. Iglakova[1], A.M. Kabanov[1], O.I. Kuchinskaya[2], G.G. Matvienko[1], V.K. Oshlakov[1], A.V. Petrov[1]

[1] Institute of Atmospheric Optics V.E. Zuev SB RAS, Tomsk, 634021, sq. Academician Zuev 1, Russia
[2] National Research Tomsk State University, Tomsk, 634050, Lenin Avenue 36, Russia
e-mail: apeximov@iao.ru, ygeints@iao.ru, zaa@iao.ru, ian@iao.ru, kam@iao.ru, koi@mail.ru, mgg@iao.ru, ovk@iao.ru, awp@iao.ru

Keywords: ultra-short laser radiation, filamentation, laser plasma
The results of numerical simulation of multiple filamentation of terawatt femtosecond pulse Ti:Sapphire laser performed on the experimental data obtained in the airway of a length of 106 m when changing the initial spatial focusing and laser power.

1. INTRODUCTION

Filamentation of laser radiation is the main regime of highpower ultrashort pulse propagation through a transparent medium [1]. Filamentation in air may stem from the spatial decay of the beam transverse profile to localised domains of high intensity – filaments, lengthy shining plasma channels arising along the propagation path, and generation of extremely wideband radiation – a supercontinuum. A recent review on filamentation of laser beams is presented in [2].

Formation of the domain with multiple filamentation at a prescribed distance from a laser source (hundreds and thousands of meters) is an important problem in femtosecond atmospheric optics, which includes both the traditional problems of remote diagnostics of atmospheric components [3] and the problems of transporting extremely high light field intensity along lengthy paths [4], creation of electroconductive channels in atmosphere [5] and laser generation of microwave radiation [6]. There are known methods for controlling the position of the filamentation domain, such as variation of the laser pulse power [7], spatial [8] and temporal focusing of ultrashort pulses [9], variation of the initial cross-section profile of the beam intensity [10] and beam size [11] including employment of adaptive manipulation [12].

The present work presents results of experimental investigations on control of the position of the filamentation domain for ultrashort pulses along lengthy atmospheric paths by varying the initial spatial focusing and pulse energy. In contrast to similar previous works [13, 14], in carrying out the experiments we have realised a complete control over the cross-section structure of the laser beam along the propagation path, which made it possible to observe the spatial evolution of high-intensity light channels formed due to the beam filamentation. The results have been used for correcting the numerical model of pulse self-action, which was used for interpreting the experimental data obtained.

2. METHODS AND RESULTS OF EXPERIMENTAL STUDY

In practice, control of filamentation of high-power radiation means providing the initiation of filamentation and, hence, plasma initiation at a prescribed distance. It is difficult to control the length of the filamentation domain due to indeterminancy of the physical processes leading to a filamentation breakdown. Perhaps, the only way to control the length of the filamentation domain is the case of tightly focused radiation where filamentation is realised within a linear focal waist of the beam [14, 15]. The principal possibility for controlling the start of filamentation itself follows from the theory of stationary self-focusing of radiation in a Kerr medium [16]. In the frameworks of this theory the expression for the length of self-focusing z_{sf} for the beam with the initial wavefront curvature f has the form

21st International Symposium on Atmospheric and Ocean Optics: Atmospheric Physics, edited by G. G. Matvienko, O. A. Romanovskii, Proc. of SPIE Vol. 9680, 96801F
© 2015 SPIE · CCC code: 0277-786X/15/$18 · doi: 10.1117/12.2205521

$$z_{sf} = \left(\frac{1}{f} + \frac{1}{z_K} \right)^{-1}, \qquad (1)$$

where z_K is the coordinate of the transverse collapse for a collimated beam (dependent on the power). For the parameter z_K there is a semi-empirical estimate that takes into account a nonstationary character of self-focusing of the radiation pulse (the Marburger formula [1]):

$$z_K = 0.367 L_D \Big/ \sqrt{\left(\sqrt{\eta} - 0.852\right)^2 - 0.0219}\,; \ \eta > 0.5 \qquad (2)$$

Here $L_d = \pi d_0^2 /(4\lambda_0)$ is the diffraction length of the radiation beam of diameter d_0 (at the level $1/e^2$) with a wavelength λ_0; $\eta = P_0 / P_c$ is the reduced power; P_0 is the initial radiation power; and P_c is the critical self-focusing power that is inversely proportional to the cube of medium polarisability.

From (1) and (2) one can see that a variation in size d_0, focal length f, or radiation power P_0 would shift the resulting length z_{sf} of beam self-focusing. The greatest effect may be observed by varying d_0 ($z_K \propto d_0^2$) and the conditions of initial focusing. In the latter case, according to (1) we see that for focused radiation ($f > 0$), beam filamentation is always realised in front of its geometrical focus, whereas under initial de-focusing of the beam ($f < 0$) the point of collapse theoretically is at infinity if the condition $|f| = z_K$ holds. Control of the start of the filamentation domain by varying the radiation power will be less efficient because the parameter P_0 in (2) is included to the power 1/2.

A scheme of experiments is shown in Fig. 1. The driving generator was a Ti:sapphire laser with the passive mode locking based on the Kerr effect. The laser source generated pulsed radiation at a centre wavelength $\lambda_0 = 800$ *nm*, with the pulse HWHM duration $t_p = 50$ *fs*, energy $E_0 \le 82$ *mJ* and peak power $P_0 \le 1.5$ *TW*. The pulse repetition rate was 10 Hz. A variable-base Galileo telescope was used as a focusing element. The focal distance for the defocusing mirror was $f_1 = -50$ *cm*, and for the focusing mirror it was $f_2 = +100$ *cm*. The beam diameter d_0 at the output of the amplifying stage was 2.5 cm and after the telescope it was $d_0 = 4$ cm.

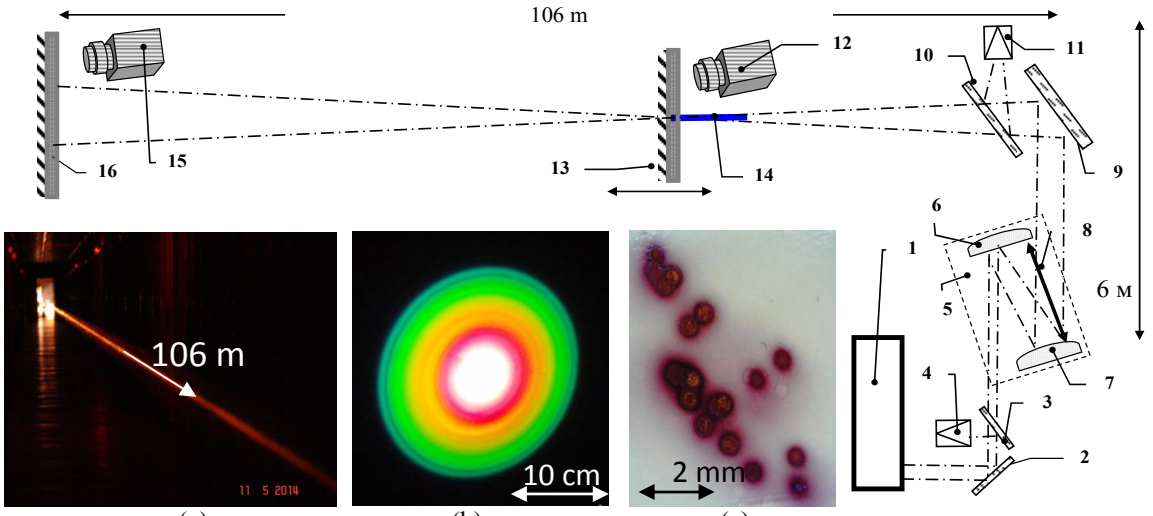

Figure 1. (a) Schematic diagram of the experiment and photographs of the laser beam cross section (filamentation at the beginning of the optical path), (b) structure of the laser beam on a screen at the end of the path and (c) burns on a photographic paper made by plasma and light channels in the filamentation domain of the path (at the centre of the circular polychromatic structure): (1) Ti:sapphire laser complex; (2, 3, 9, 10) turning plates; (4) pulse duration meter (autocorrelator); (5) Galileo telescope; (6) defocusing mirror; (7) focusing mirror; (8) variable base of the telescope; (11) OPHIR-II pulse energy meter; (12, 15) CCD-cameras, photographic or video cameras; (13) sliding screen; (14) filamentation domain; (16) fixed screen.

Figures 2 and 3 present the results of measurements of the spatial position of the filamentation domain for ultrashort pulses, which demonstrate the ways of controlling filamentation by varying the initial spatial focusing and the

laser pulse energy. The boundaries of the path segments where plasma channels arose and accompanied beam filamentation were determined by presence/absence of the characteristic thermal burns on a photographic paper (glossy, colour, contrast, TU 6-17-766-76), such as, for example, those shown in Fig. 1c. Each point in Figs 2 and 3 is an arithmetic mean over ten independent measurements of the coordinates of the filamentation domain.

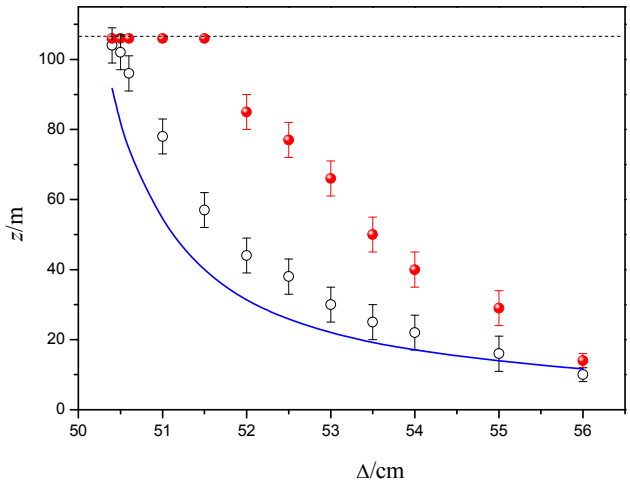

Figure 2. Coordinates of the beginning (○) and end (●) of the filamentation domain (E_0 = 60 mJ, d_0 = 4 cm) vs. the length of the telescope base D (focal length). Dashed curve refers to the boundary of the optical path, solid curve corresponds to the calculation by formula (1).

From Fig. 2 one can see that an increase in the telescope base by several centimetres, which corresponded to a reduction of the effective focal length f to ~12 m and, hence, to an increase in sharpness of radiation focusing, makes it possible to move the filamentation domain along the entire 100-metre long path. Note that at the distance between mirrors $\Delta < 52$ cm, when the laser beam was almost collimated, beam filamentation originated in the second half of the path, and it was impossible to determine the far boundary of existence for the plasma channel domain.

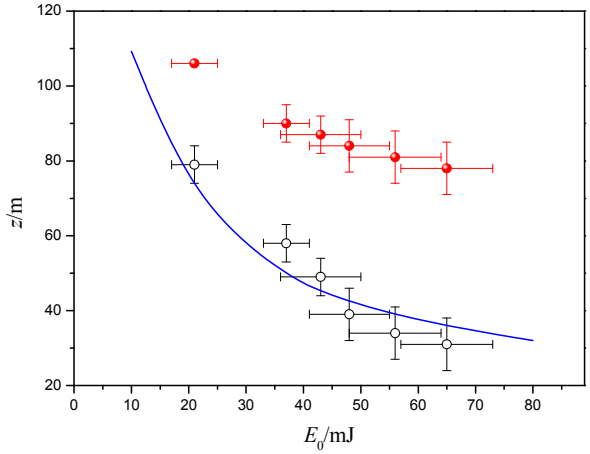

Figure 3. Coordinates of the beginning (○) and end (●) of the filamentation domain for the collimated beam with d_0 = 2.5 cm vs. the laser pulse energy E_0. Solid curve corresponds to the calculation by formula (2).

Measurement results of the spatial boundaries of the plasma initiation domain when the initial energy (peak power) of laser pulses was varied are shown in Fig. 3. Here, a narrower laser beam was used (without a telescope) in order to bring the filamentation domain nearer and arrange it within the optical path at low pulse energies. One can see that the variation in the radiation energy also leads to changes (predicted by theory) in the beginning of the filamentatioin domain, namely, to an earlier start of filamentation at increased energy E_0. Also, results of the theoretical estimates for the self-focusing length z_{sf} performed by formula (2) are presented in Fig. 3. A satisfactory agreement with experimental points is observed at the specified critical power P_c = *15 GW*. This value is higher than the value of 3–5 GW

conventionally used for air [11, 13, 14]; however, it correlates with the results of recent work [17] obtained on the basis of more accurate measurements of cubic nonlinearity of atmospheric gases [18].

Similarly, the solid curve in Fig. 2 is obtained in the case of varied focal length f of the telescope at a constant laser pulse energy E_0. The values of the telescope base Δ were translated to the effective focal length by the known formula $f = f1\ f2/(f1 + f2 - \Delta)$. A theoretical estimate of the self-focusing length z_{sf} (2) also satisfactorily corresponds to the measured distances to the start of the beam filamentation domain.

There is one more important circumstance that should be taken into account in practical realisation of the two methods for controlling the filamentation domain of radiation. From analysis of Figs 2 and 3 it follows that the start of the filamentation domain can be equally efficiently realised by focusing the beam or by varying its energy. However, these two methods differently affect the position of the far boundary of the filamentation domain, that is, the filamentation length. Tighter focusing makes the position of the filamentation start closer and simultaneously shortens the length of the domain of plasma channel existence along the path, whereas a greater laser pulse power, giving the same result for the filamentation start, has an opposite effect on its length, making it longer.

The physical background is clear, because geometrical focusing of the beam changes its angular divergence, which is of particular importance for maintaining filamentation after the beam crosses the linear focal waist. In the conditions of tight focusing, the geometrical divergence of radiation may overcome the Kerr self-focusing and destabilise or break the process of filamentation behind the linear focus of the beam [19, 20].

If, all other factors being equal, the laser power is varied, then the coordinate of the nonlinear focus z_K (2) will shift and, hence, the resulting length of self-focusing z_{sf} will change. In this case the length of the filamentation domain will be mainly determined by the radiation energy, that is, by the possibility of the whole laser beam to serve as an energy container for the domains subjected to filamentation and to compensate for energy losses to plasma initiation.

In addition to manipulations with longitudinal position of the filamentation domain we have also analysed the transverse structure of the radiation channel in this domain. We were interested in the number of fixed plasma channels N_p and its variation along the path. The number of plasma channels in the laser beam cross section was found by calculating the number of contrast burns left on a photographic paper placed at various distances along the optical path. One such result is shown in Fig. 4 for the collimated beam at the maximal realised pulse energy. One can see that the parameter N_p is nonmonotonic along the filamentation domain. At first, only several burns are observed, then its number increases to approximately twenty near the geometrical centre of the filamentation zone, and finally the number of burns again reduces to the end of the zone. Since there was no initial beam focusing, the extremum in the dependence of the number of plasma channels on the coordinate along the propagation path seems to be related with the origin of the nonlinear focus of the entire beam in this region [21], which provides the maximal concentration of the radiation energy in the beam cross section. This circumstance favours the development of smallscale self-focusing and filamentation of radiation possessing a supercritical power ($\eta >> 1$).

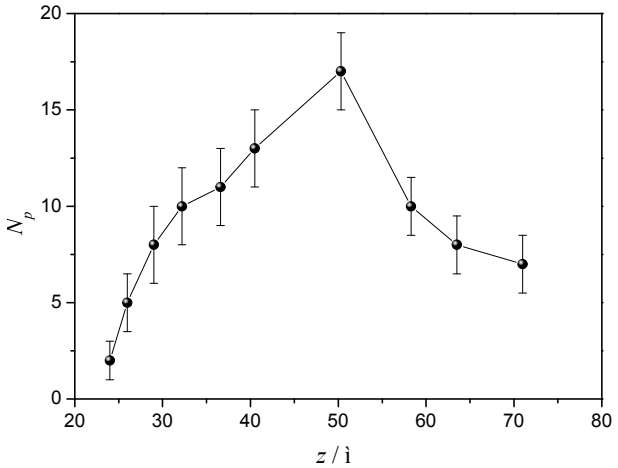

Figure 4. Number of plasma channels in the cross section of the laser beam with the pulse energy E_0 = 82 mJ along the path.

3. RESULTS OF THEORETICAL SIMULATION

In order to understand the physical processes inherent in the properties obtained experimentally, we have numerically simulated the self-action of a high-power ultrashort pulse in an optically nonlinear air medium. Theoretical consideration of this problem is usually based on the paraxial quasi-optical equation written either for the frequency spectrum of the field [22] or for the time profile of the electric field envelope of a light pulse [1]. In the latter case this equation in the literature is termed the nonlinear Schrödinger equation (NLSE). The entire problem of describing multiple filamentation of a laser pulse requires calculation of the spatial dynamics of the optical field in all four coordinates: three spatial and one time coordinates. A numerical solution of this complete four-dimensional selfaction problem for the laser beams having a diameter of several centimetres corresponding to the experimental conditions would require a huge computer memory and extremely cumbersome computations, which in current conditions cannot be reached even with high-productivity server clusters [23]. For this reason, in simulating the nonlinear propagation of wide-aperture laser radiation we used the so-called reduced NLSE version that is obtained by integrating over time coordinate.

This approach was suggested in [24] and demonstrated a good agreement of data, first of all, concerning the position of the nonlinear focus and the length of the filamentation zone, with results of solving the complete problem that takes into account a temporal pulse structure. Clearly if the time coordinate is excluded from the numerical simulation, then one cannot correctly take into account the 'time memory' of a propagation medium that is related to frequency dispersion of the time profile of a light pulse, the inertial character of cubic nonlinearity (combination self-scattering) and the nonstationary plasma defocusing. However, the employment of the stationary version of the NLSE is justified in modelling atmospheric propagation of high-power radiation in the conditions of acting random factors (turbulence [25], aerosol attenuation [26]), which lead to a stochastic character of the beam intensity profile and to development of chaotic small-scale self-focusing and filamentation (optical turbulence [27]). In this case, the theoretical results should not necessarily repeat the spatial-temporal intensity profile of the laser beam; those should only reliably describe evolution of averaged (effective) characteristics of the beam.

In the experiments discussed, the influence of random atmospheric factors was minimised by arranging the laser path in enclosed space with stable thermodynamic parameters (experiments were performed at night). However, the radiation itself had certain instability while entering the path. This concerned both the transverse structure of the beam that changed its configuration from run to run and the pulse energy that might vary within ten percent. That is why the initial profile of the laser beam was prescribed in numerical simulations by a model super-Gaussian beam $u_G(\mathbf{r}_\perp)$ with added amplitude noise of the light field:

$$u(\mathbf{r}_\perp, z=0) = \left[u_G(\mathbf{r}_\perp) + A\tilde{u}_{rnd}(\mathbf{r}_\perp)\right].$$

Here $u(\mathbf{r}_\perp, z)$ is the normalised complex amplitude of the electric field of a light pulse, which is a function of transverse coordinates $\mathbf{r}_\perp$ and of the evolution variable z; $u_G = \exp\left\{-\left(8|\mathbf{r}_\perp|/d_0\right)^4\right\}\exp\left\{-i\left(2k_0|\mathbf{r}_\perp|^2/f\right)\right\}$; d_0 is the diameter at a level $1/e^2$; f is the initial radius of curvature of the wavefront of radiation; and $\tilde{u}_{rnd}$ is the amplitude of noise with normal distribution, zero average value and peak amplitude A.

In the normalised variables $\mathbf{r}_\perp \to 2^{3/2}\mathbf{r}_\perp/d_0$ and $z \to z/L_R$, the evolution equation of the average (over time) amplitude of the optical field $u(\mathbf{r}_\perp, z)$ has the form [28]

$$\left\{\frac{\partial}{\partial z} - \frac{i}{4}\nabla_\perp^2 - i\sum_{m=1}^{M}\frac{L_R}{L_{2m}}|u|^{2m} + \frac{1}{2}\frac{L_R}{L_W}\overline{W}_I\left(|u|^2\right)\frac{(1-B)}{|u|^2} + \frac{i}{2}\frac{L_R}{L_{pl}}\left(1 - \frac{i}{\omega_0\tau_c}\right)B + L_R\frac{\alpha_L}{2}\right\}u = 0, \quad (3)$$

The linear part of this equation makes allowance for beam diffraction and linear absorption of radiation in the medium with a volume absorption coefficient α_L. The model of air optical nonlinearity takes into account cubic (the Kerr effect) and higher-order field nonlinearities as well as variation in a complex refractive index of the medium due to photo-ionisation of air. The following notations are used in (3): $\nabla_\perp^2$ = is the transverse Laplacian; $L_R = 0.5L_d$ is the

Rayleigh length of the beam; $k_0 = 2\pi/\lambda_0$ is the wavenumber; $L_{2m} = \left(k_0 n_{2m} I_0^m\right)^{-1}$ is the characteristic length of the *m*th order (*m* = *1,...,M*) optical nonlinearity; n_{2m} is the nonlinear surplus to the refractive index;I_0 is the initial (average) pulse intensity; $\bar{W}_I = W_I\left(|u|^2\right)\Big/W_I\left(I_0\right)$ is the relative rate of photo-ionisation of the air medium; $L_W = I_0/\left(\rho_{nt} W_I(I_0)\Delta E_i\right)$ is the characteristic length of multi-photon absorption in the medium with the initial concentration of neutral particles ρ_{nt} and potential of single ionisation ΔE_i ; $L_{pl} = \left(\sigma_c \rho_{nt} \omega_0 \tau_c\right)^{-1}$ is the characteristic length of radiation defocusing in plasma; ω_0 is the centre frequency of the radiation pulse; σ_c is the cross section of inverse-bremsstrahlung absorption; and τ_c is the average time of the electron free path.

The coefficient *B* makes allowance for the cumulative action of plasma nonlinearity formed to the end of the radiation pulse due to the direct field and impact (cascade) ionisation of medium molecules:

$$B(u) = \frac{W_I\left(I_0|u|^2\right)}{W_I - \nu_{cas} I_0 |u|^2} + \left(1 - \mathrm{e}^{-t_0\left(W_I - \nu_{cas} I_0 |u|^2\right)}\right)\left[\frac{\bar{\rho}_e^0}{t_0\left(W_I - \nu_{cas} I_0 |u|^2\right)} - \frac{W_I\left(I_0|u|^2\right)}{t_0\left(W_I - \nu_{cas} I_0 |u|^2\right)^2}\right]$$

where $\nu_{cas} = \sigma_c/\Delta E_i$ is the coefficient of molecule cascade ionisation; $\bar{\rho}_e^0 = \rho_e^0/\rho_{nt}$; and ρ_e^0 is some initial concentration of electrons in the medium (usually it is ~10^4 m^{-3} [29]). The adjustable parameter t_0 in this expression is chosen from the range $0 < t_0 \le t_p$, where t_p is the initial laser pulse duration (HWHM). As a rule, the value $t_0 = 0.1 \cdot t_p$ sufficiently well takes into account the characteristic time-domain compression of the pulse, which occurs in the Kerr medium in front of the nonlinear focus.

In numerical simulations, the following parameters were taken for the laser radiation at the carrier wavelength λ_0 = 800 nm: t_p = 60 fs, *A* = 0.2, n_2 =1.2×10^{-19} cm^2 W^{-1} [30], n_{2m} = 0 for *m* > 2, α_L = 0, ρ_{nt} = 2.6×10^{25} m^{-3}, σ_c = 5.5×10^{-20} cm^{-2}. The photo-ionisation rate W_i was calculated according to the well-known Popov –Perelomov–Terent'ev model of ionization [31] for a synthetic air medium (79% N2 and 21% O2) with the ionisation potential ΔE_i =14.1 eV. The initial pulse intensity I_0 was determined from real characteristics of radiation by the formula $I_0 = 8E_0\Big/\left(t_p \pi d_0^2\right)$.

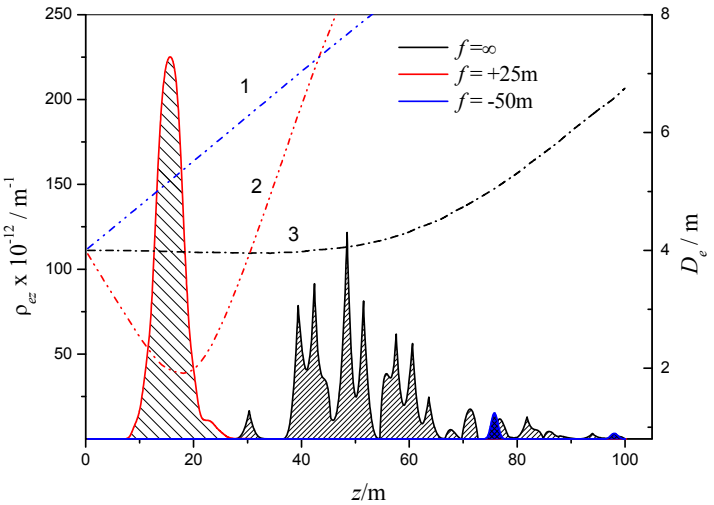

Figure 5. Path evolution of the linear concentration of free electrons (shaded areas) generated due to filamentation of the laser beam with E_0 = 80 mJ and d_0 = 4 cm and effective diameter D_e (curves) at *f* = (1) –50 and (2) +25 m; (3) collimated beam.

Figure 5 presents the results of the numerical simulation of the linear concentration ρ_{ez} of the plasma domain along the propagation path of the laser beam with the initial intensity E_0 = 80 mJ and diameter d_0 = 4 cm under the varied initial focusing given by the parameter of the radiation wavefront curvature *f*. The linear concentration of free electrons generated under the action of the laser pulse was determined by integrating numerically the volume concentration of electrons $\rho_e(\mathbf{r}_\perp, z)$ over the whole space of the transversal grid: $\rho_{ez}(z) = \iint_{\mathbf{R}_\perp} \rho_e(\mathbf{r}_\perp, z)\, d\mathbf{r}_\perp$. In turn, for obtaining the volume concentration of plasma the following expression was used (with only the field ionisation taken into account):

$$\rho_e(\mathbf{r}_\perp, z) = \rho_{nt}\left[1 - \exp\left\{-W_I\left(I_0\left|u(\mathbf{r}_\perp, z)\right|^2\right)t_0\right\}\right].$$

In calculations, the initial focusing was chosen in wider limits than it was possible in real measurements and included negative values of the focal length *f* of the optical system, which corresponded to the case of radiation with initial angular divergence (the case of defocusing).

As one can see in Fig. 5, the concentration of the plasma channel integrated over the cross section is distributed nonuniformly along the path and demonstrates local spikes of the parameter ρ_{ez} at some places. These spikes may be identified with the corresponding increase in the number of plasma channels N_p accompanying each separate filament of the light beam. Indeed, since the peak volume concentration of free electrons ρ_e in each plasma channel is limited due to a similar fundamental limitation of the peak intensity in a filament [32], an increase or decrease of linear concentration ρ_{ez} denotes the corresponding increase or decrease in the number of plasma channels (and filaments) at particular places of the optical path.

As in experiments, variation in the focal length *f* shifts the start of the filamentation domain: the focusing makes it closer to the beginning of the path and defocusing makes it farther. However, structural changes of the linear concentration of the plasma channel are also observed in this case. If a collimated beam (with no focusing) is compared with the beam that was initially focused, then one can see that in the latter case the length of the plasma domain is noticeably shorter and the absolute value of ρ_{ez} is greater, which testifies that the number of filaments increases when radiation is focused. In the focused beam, the maximal concentration ρ_{ez}, and, hence, the maximal number of filaments N_p is observed in the nonlinear focus that is determined by the minimal root-mean-square (effective) diameter D_e of the beam as a whole [21]:

$$D_e(z) = 2\left[t_p / E(z) \iint_{\mathbf{R}_\perp} d^2\mathbf{r}_\perp I(\mathbf{r}_\perp, z)\left|\left(\mathbf{r}_\perp - \mathbf{r}_{gr}\right)\right|^2\right]^{1/2},$$

where $E(z)$ is the radiation energy, and $\mathbf{r}_{gr}$ is the radius-vector of the beam centre-of-mass (by intensity). Dependences $D_e(z)$ are also presented in Fig. 5.

In the case of collimated radiation, plasma is distributed along the more extended part of the path with the length of ~50 m and is characterised by a strong variation in amplitudes of local maxima of the linear density. Considering the behaviour of the light beam from the viewpoint of its effective size one may conclude that the beam remains collimated to the distance of up to ~48 m, which can be considered the nonlinearfocal length;then the beam steadily expands. Generation of plasma channels and, consequently, beam filamentation in this case do not stop.

Filamentation of radiation with initial divergence ($f < 0$) occurs at distances longer then in the case of collimated radiation and is accompanied by a noticeable increase in the beam size. The effective diameter D_e of the defocused beam evolves without forming a nonlinear focus; however, this does not prevent the development of small-scale self-focusing and filamentation in some parts of the beam. At the focal length of the optical system *f* = –50 m (Fig.

5) a numerical calculation yields the start of filamentation at a distance of ~75 m, which actually is thrice longer than the length of self-focusing for the collimated beam.

The coordinate z_m of the absolute maximum of distribution $\rho_{ez}(z)$ and the length of the region of active plasma initiation L_p are presented in Fig. 6 for various variants of beam focusing. The parameter L_p is calculated as the difference between the coordinate extremes corresponding to the condition $\rho_{ez} \geq \rho^*$, where $\rho^* = 10^{12}$ m^{-1}. A certain freedom in choosing the value of ρ^* is inevitable because the threshold concentration of the plasma channel at which the photographic paper burns is not known in measurements. Note that in our numerical simulations, overrunning the characteristic level ρ^* approximately corresponded to the peak value of the volume concentration of free electrons ~10^{20} m^{-3}.

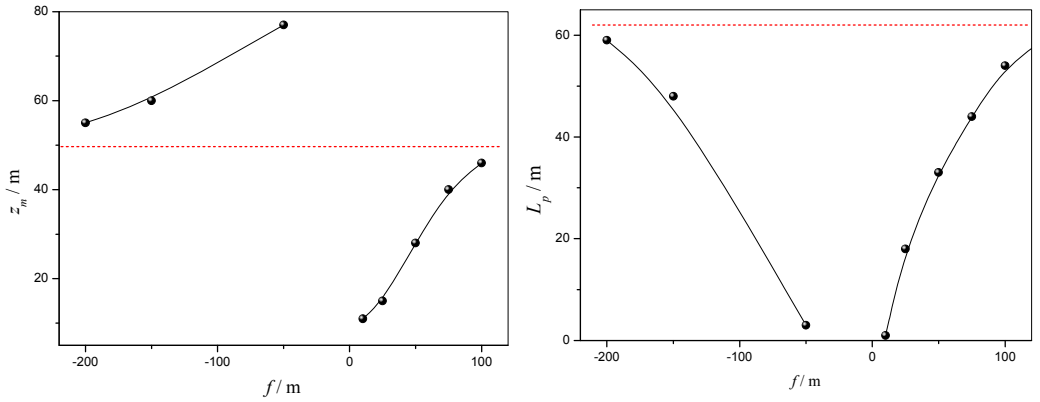

Figure 6. Coordinate of (a) the absolute maximum zm and (b) the length of the filamentatioin domain Lp vs. the focal length f. Dashed lines correspond to collimated radiation.

According to calculations, the general feature of filamentation of focused or defocused radiation is a shorter filament length as compared to the filament formed upon self-focusing of the collimated beam. The reason is a greater angular divergence of radiation with a non-plane phase front, which manifests itself either at the beginning of the path (the case of defocusing) or behind the nonlinear focus (the case of a focused beam). A stronger angular divergence reduced the efficiency of an energy 'feed' of filaments by peripheral 'nonfilamented' zones of the beam, which results in the development of unstable filamentation and an earlier breakdown of plasma channels.

Figure 7 shows the transverse profiles of the volume concentration ρ_e of the plasma channel formed in the light beam at points z_m of a maximal linear concentration of plasma. The profiles were obtained by solving numerically the reduced NLSE (3) for the beam with an initial noisy multimodal intensity distribution.

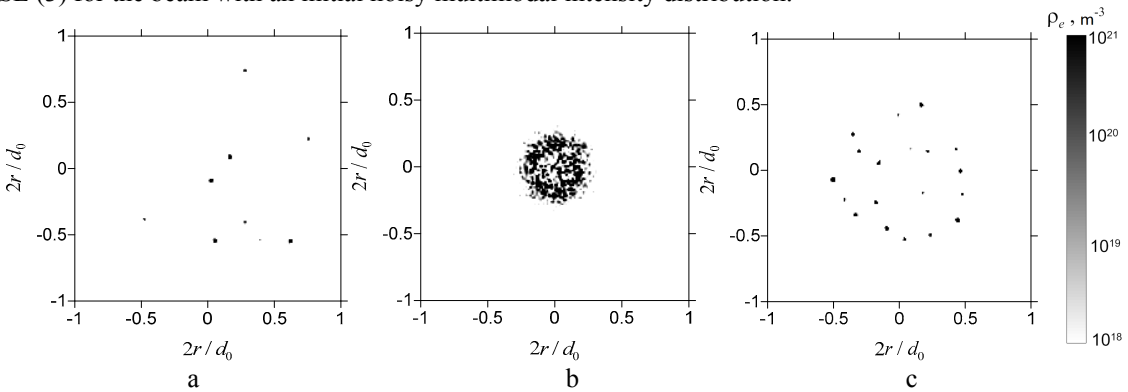

Figure 7. Cross-section profile of the volume concentration re of a plasma channel in the case of laser beam filamentation with E_0 = 80 mJ and d0 = 4 cm for f = (a) –150 and (b) +25 m; (c) collimated beam.

In the figure one can see that the variation in the wavefront curvature attained due to the variation of the focal length of the optical system results in substantial changes of the cross-section profile of concentration in the plasma domain. Collimated and focused beams are characterised by a sufficiently dense distribution of separate plasma channels (and filaments) over the cross section (Figs 7b and 7c), whereas the strongly defocused radiation (Fig. 7a) is characterised by a greater spatial spread. As shown in [13], this circumstance may substantially affect the effective electrical conduction of formed plasma channels, which is extremely important in problems, for example, of laser control of electric discharges in atmosphere [33].

4. CONCLUSIONS

The results of conducted experiments show the real possibility to control the spatial position of the domain of multiple filamentation and plasma initiation of a high-power ultrashort pulse propagating along a 100-metre air path. The control was realised both by varying the initial spatial focusing of the beam and by changing the energy of the initial radiation pulse. In the first case, at a stronger focusing the domain of filamentation starts closer to the beginning of the optical path and simultaneously its length becomes shorter. In the case of increasing the pulse energy at constant focusing, the earlier start of filamentation/plasma initiation is observed, and the length of the filamentation domain increases.

More than ten simultaneous plasma channels have been experimentally observed that were formed in a cross section of the laser beam with a unimodal character of their distribution along the optical path. Numerical simulation of the self-action of high-power pulsed radiation in an optically nonlinear air medium performed by the reduced NLSE has shown that the spatial position of the maximal number of plasma channels in the cases of focused or collimated radiation correlates with the coordinate of nonlinear focus of the beam as a whole and, hence, can also be efficiently controlled. Calculations performed for a preliminarily defocused beam show that filamentation occurs at substantially longer distances than in the case of a collimated beam and is accompanied by a noticeable increase in the size of the laser beam in the zone of active plasma initiation.

This work was financially supported by the Russian Science Foundation (agreement № 15-17-10001).

REFERENCES

[1] Shen Y.R., Boyd R.W., Lukishova S.G. (Eds) Self-Focusing: Past and Present (New York–Berlin: Springer, 2009).
[2] Houard A., Liu Y., Mysyrowicz A. J. Phys. Conf. Ser., 497, 012001 (2014).
[3] Rairoux P., Schillinger H., Niedermeier S., Rodriguez M., Ronneberger F., Sauerbrey R., Stein B., Waite D., Wedekind C., Wille H., Wöste L. Appl. Phys. B, 71, 573 (2000).
[4] Béjot P., Bonacina L., Extermann J., Moret M., Wolf J.P., Ackermann R., Lascoux N., Salamé R., Salmon E., Kasparian J., Bergé L., Champeaux S., Guet C., Blanchot N., Bonville O., Boscheron A., Canal P., Castaldi M., Hartmann O., Lepage C., Marmande L., Mazataud E., Mennerat G., Patissou L., Prevot V., Raffestin D., Ribolzi J. Appl. Phys. Lett., 90, 151106 (2007).
[5] Khan N., Mariun N., Aris I., Yeak J. New J. Phys., 4, 61 (2002).
[6] Cheng C.C., Wright E.M., Moloney J.V. Phys. Rev. Lett., 87, 213001 (2001).
[7] Mechain G., Amico C.D., Andre Y.-B., Tzortzakis S., Franco M., Prade B., Mysyrowicz A., Couairon A., Salmon E., Sauerbrey R. Opt. Commun., 247, 171 (2005).
[8] Fibich G., Sivan Y.,Ehrlich Y.,LouzonE.,FraenkelM.,Eisenmann S., Katzir Y., Zigler A. Opt. Express, 14, 4946 (2006).
[9] Nuter R., Skupin S., Bergé L. Opt. Lett., 30, 917 (2005).
[10] Kandidov V.P., Akozbek N., Scalora M., Kosareva O.G., Nyakk A.V., Luo Q., Hosseini S.A., Chin S.L. Appl. Phys. B, 80, 267 (2004).
[11] Kosareva O.G., Panov N.A., Akozbek N., Kandidov V.P., Luo Q., Hosseini S.A., Liu W., Gravel J.-F., Roy G., Chin S.L. Appl. Phys. B, 82, 111 (2006).
[12] Ackermann R., Salmon E., Lascoux N., Kasparian J., Rohwetter P., Stelmaszczyk K., Li S., Lindinger A., Wöste L., Béjot P., Bonacina L., Wolf J.-P. Appl. Phys. Lett., 89, 171117 (2006).

[13] Apeksimov D.V., Geintz Yu.E., Zemlyanov A.A., Kabanov A.M., Matvienko G.G., Stepanov A.N. Opt. Atmos. Okeana, 25, 929 (2012).
[14] Geints Yu.E., Zemlyanov A.A., Kabanov A.M., Matvienko G.G., Stepanov A.N. , Quantum Electron., 43, 350 (2013).
[15]. Geints Yu.E., Zemlyanov A.A., Ionin A.A., Kudryashov S.I., Seleznev L.V., Sinitsyn D.V., Sunchugasheva E.S. Zh. Eksp. Teor. Fiz., 138, 822 (2010).
[16] Akhmanov S.A., Sukhorukov A.P., Khokhlov R.V. Usp. Fiz. Nauk, 93, 19 (1967).
[17] Polynkin P., Kolesik M. Phys. Rev. A, 87, 053829 (2013).
[18] Wahlstrand J.K., Cheng Y.-H., Milchberg H.M. Phys. Rev. A, 85, 043820 (2012).
[19] Talebpour A., Petit S., Chin S.L. Opt. Commun., 171, 285 (1999).
[20] Geints Yu.E., Zemlyanov A.A. Laser Phys., 23, 035301 (2013).
[21] Zemlyanov A.A., Geints Yu.E. Opt. Spektrosk., 104, 852 (2008).
[22] Kolesik M., Moloney J.V., Mlejnek M. Phys. Rev. Lett., 89, 283902 (2002).
[23] Shlenov S.A., Bezborodov A.E., Smirnov A.V., Proc. Conf. on Parallel and Distributed Processing Techniques and Applications 4003, 94–98 (2006).
[24] Bergé L., Skupin S., Lederer F., Méjean G., Yu J., Kasparian J., Salmon E., Wolf J.P., Rodriguez M., Woste L., Bourayou R., Sauerbrey R. Phys. Rev. Lett., 92, 225002 (2004).
[25] Salamé R., Lascoux N., Salmon E., Ackermann R., Kasparian J., Wolf J.-P. Appl. Phys. Lett., 91, 171106 (2007).
[26] Silaeva E.P., Kandidov V.P. Opt. Atmos. Okeana, 22, 132 (2009).
[27] Mlejnek M., Kolesik M., Moloney J.V., Wright E.M. Phys. Rev. Lett., 83, 2938 (1999).
[28] Geints Yu.E., Zemlyanov A.A. J. Opt. Soc. Am. B, 31, 788 (2014).
[29] Raizer Yu.P. Gas Discharge Physics (Berlin: Springer, 1991; Moscow: Nauka, 1987).
[30] Loriot V., Hertz E., Faucher O., Lavorel B. Opt. Express, 18, 3011 (2010).
[31] Perelomov A.M., Popov V.S., Terent'ev M.V. Zh. Eksp. Teor. Fiz., 50, 1393 (1966).
[32] Becker A., Akozbek N., Vijayalakshmi K., Oral E., Bowden C.M., Chin S.L. Appl. Phys. B, 73, 287 (2001).
[33] Rodriguez M., Sauerbrey R., Wille H., Wöste L., Fujii T., André Y.-B., Mysyrowicz A., Klingbeil L., Rethmeier K., Kalkner W., Kasparian J., Salmon E., Yu J., Wolf J.-P. Opt. Lett., 27, 772 (2002).